https://doi.org/10.5194/egusphere-2026-1578
Preprint. Discussion started: 22 April 2026

Impact of large-scale atmospheric winter circulation on sea ice motion in the Arctic in 2000-2025

Ilona Välisuo [1], Tiina Nygård[1]

[1]Finnish Meteorological Institute, Meteorological Research, Helsinki, 00560, Finland

Correspondence to: Ilona Välisuo (ilona.valisuo@fmi.fi)

Abstract.

This study examines the relationship between atmospheric large-scale circulation indices, twelve finer-scale circulation types, and ice drift speed at three fixed transects. The aim is to analyse the impact of atmospheric pressure patterns on ice drift. The North Atlantic Oscillation (NAO), Arctic Oscillation (AO), Pacific-North American Pattern (PNA), and Arctic Dipole Anomaly (DA) explain about 10% of the drift speed variations in the Beaufort Gyre (BG), Transpolar Drift Stream (TDS) and Fram Strait (FR). Self-organizing maps (SOM) analysis further reveals distinct circulation types even when large-scale circulation indices appear similar, which explains the low explanatory power of the large scale circulation indices alone. However, mean sea level pressure (MSLP) variability at optimal locations accounts for approximately 40 to 60% of the observed drift speed variations, with sea ice thickness and thickness anomalies showing no significant improvement in explanatory power. Sea ice thickness exhibits a strong seasonal cycle and is predominantly influenced by the time of year, suggesting that its impact on drift speed may manifest over climatic timescales.

1 Introduction

Arctic sea ice plays a key role in the climate system. Sea ice and snow reflect up to approximately 85% of the solar radiation away from the surface (Perovich and Polashenski, 2012). Sea ice insulates the ocean from the atmosphere and prevents heat exchange between the water and air. Arctic sea ice is also a reservoir of fresh water, and ice growth and melting affect the salinity of the surface layer of the ocean. Furthermore, sea ice is a habitat for life forms ranging from microorganisms to large marine mammals. Due to climate warming, the Arctic is losing ice in all measures: area, concentration, thickness, and age. Decreasing concentration and thickness make ice more responsive to wind forcing, and the Arctic sea ice drift speed has increased since 1979. This increased mobility has been attributed to thinner sea ice and changes in wind (Olason and Notz, 2014). Furthermore, researchers on the MOSAIC-drifting station observed that sea ice dynamic deformations in winter were more important than expected, possibly due to younger and thinner ice than during previous winter expeditions (Nicolaus et al., 2022).

The Arctic sea ice shows semi-permanent drift patterns: anticyclonic circulation in the Beaufort Sea region called the Beaufort Gyre (BG) and the Transpolar Drift Stream (TDS), which transports ice from the Siberian shelf across the Arctic towards the Fram Strait and the Atlantic. Climatological atmospheric pressure patterns create winds that drive ice motion in the Beaufort Gyre, Transpolar Drift Stream, and Fram Strait (Meredith et al., 2019). Ice motion is essential for redistributing and exporting ice from the Arctic. Ice transport affects the local sea ice concentration and thickness, which are important preconditions for ice formation in the next season, and it affects the predictability of sea ice (Guemas et al., 2014).

The leading modes of northern Hemisphere atmospheric variability are the North Atlantic Oscillation (NAO), Arctic Oscillation (AO), Pacific-North American Pattern (PNA), and Arctic Dipole Anomaly (DA). Atmospheric circulation indices describe atmospheric pressure patterns, which in turn define the geostrophic wind field. As a rule of thumb, the geostrophic wind explains approximately 50% of the ice drift speed variability (Colony and Thorndike, 1984). Armitage et al. (2018) showed that the AO, the leading mode of Arctic (20 to 90°N) atmospheric pressure variability, is connected to the ice drift

https://doi.org/10.5194/egusphere-2026-1578
Preprint. Discussion started: 22 April 2026

speed and direction at Arctic coastal shelf regions: the ice drift appears cyclonic circulation for AO+, and anticyclonic for AO–. The NAO, the leading mode of Euro-Atlantic atmospheric variability, is closely related to the AO. The NAO has been linked especially to ice export via the Fram Strait. A deep Icelandic Low pressure in positive NAO years favours southward ice flux through the Fram Strait (Kwok and Rothrock, 1999). Further studies have shown that a pressure dipole between the east and west Arctic, often referred to as the Arctic Dipole Anomaly (DA), is an essential driver of ice export via the Fram Strait. Vihma et al. (2012) presented the Central Arctic Index (CAI), which describes the pressure gradient between the Canada Basin and Laptev Sea. CAI is more strongly related to the sea ice drift speed in the TDS than DA, highlighting the role of regional pressure patterns.

Here, we studied the Arctic atmospheric circulation types, that is, pressure patterns that reveal more details of atmospheric conditions than the circulation indices. We investigated how the circulation types impact and control sea ice motion in the current climate. We used self-organising maps (SOM) to cluster the mean sea level pressure (MSLP) fields into circulation types. An advantage of the SOM method compared to circulation indices is its flexibility in two-dimensional space. It can easily be adopted to the region of interest, and it captures the zonal and meridional variability at the same time (Nygård et al., 2023). The AO, for example, is strongly dominated by the north-south pressure variability, and the DA is an east-west-variability index. Further, the SOM methods is more suitable for studying the synoptic scale variations in the atmospheres, than the large-scale indices. Hordoir et al., (2026) demonstrate that the change in synoptic frequency, in their case the change in the transition timescale of low-pressure systems over the North Sea, is a key driver of oceanic flow in the Barents Sea opening. All in all, the SOM methods provide a tool to aggregate atmospheric information, without losing the relevant spatiotemporal details. We analysed how the SOM-based circulation types were related to the NAO, PNA, AO, and DA. Furthermore, we linked the ice drift speed anomalies to the circulation types. We hypothesise that the large-scale circulation indices average out local variations in the atmospheric pressure field and are thus not optimal tools for understanding the atmosphere – sea ice linkages in the Arctic. Tsukernik et al., (2010) showed that NAO is not the most dynamically relevant pattern for explaining the variations in sea ice motion through Fram Strait. Heukamp et al. (2023) stated that the synoptic cyclones modulated the impact of NAO on ocean transport in the Barents Sea Opening. In addition, we see that the DA, which describes the local atmospheric conditions, is a better explanator for sea ice transport in the Arctic than the AO or NAO. All this signals, that large-scale circulation indices do not capture all the essential atmospherics drivers of large scale sea ice motion.

A new aspect of this study is the use of SOM clustering to study the linkages between the Mean Sea Level Pressure (MSLP) and ice drift speed. We also show correlation maps of ice speed and MSLP to identify the most relevant pressure patterns linked to the BG, TDS, and FR. For the FR, our results are similar to those of Tsukernik et al. (2010). We also used linear regression models to study the connections between ice drift speed and NAO, AO, DA, and PNA.

2 Material and Methods

This study builds on the ERA5 reanalysis (Hersbach et al., 2020), Polar Pathfinder ice motion data (Tschudi et al., 2019), and atmospheric circulation indices, of which AO, NAO, and PNA were provided by the NOAA Climate Prediction Center (CPC), and DA was calculated based on ERA5. We identified twelve typical circulation types using SOM analysis and calculated the average ice drift speed for these circulation types. We analysed the ice drift speed at transect locations that represent ice motion in the BG, TDS, and FR. The results highlight that the locations of cyclones and anticyclones are essential modulators of ice speed and direction. The data and methods are described in detail in Sections 2.1 to 2.5.

https://doi.org/10.5194/egusphere-2026-1578
Preprint. Discussion started: 22 April 2026

2.1 ERA5 Atmospheric reanalysis

We used the mean sea level pressure (MSLP) fields from the ERA5 reanalysis (Hersbach et al., 2020) to perform self-organising map (SOM) -clustering, calculate the Arctic Dipole Anomaly (DA) -index, and show the spatial correlation between ice motion and atmospheric pressure. We retrieved the daily means of 1-hourly data for the Northern Hemisphere. The original spatial resolution of the data was 0.25°. We interpolated the data to a 50 km × 50 km equal area grid (EASE2) for the SOM analysis, but we used the original resolution for other analyses and for plotting. We downloaded the data from the Copernicus Climate Data Store.

2.3 Polar Pathfinder Sea Ice Motion

We used daily ice motion vectors from the Polar Pathfinder Daily 25 km EASE-Grid Sea Ice Motion Vectors, Version 4 dataset (Tschudi et al., 2019). The Polar Pathfinder ice motion vectors were generated from a composite of satellite remote sensing, sea ice buoy, and reanalysis data. The data cover both polar regions, and here we used data from the Northern Hemisphere (29.7°N to 90°N). The temporal resolution was daily and the horizontal resolution was 25km × 25 km. We used data from December 2000 to 31 December 2023 which is the last available day in the dataset.

2.3 Circulation indices

Circulation indices describe large-scale atmospheric pressure and circulation patterns. At its simplest, the circulation indices can be estimated by the atmospheric pressure difference between two locations. A standard method to calculate circulation indices is the Empirical Orthogonal Function Analysis, which allows the reduction of the dimensionality of the spatial-temporal dataset and express it in terms of variances (Wilks, 2011). Below, we describe the circulation indices used in this study and the methods used to calculate them.

2.3.1 Arctic Oscillation

The AO is the leading structure of sea level pressure (SLP) variability over the Arctic. It depicts a zonally symmetric pressure pattern with a primary centre of action over the central Arctic and opposing pressure anomalies at mid-latitudes. A positive AO indicates a lower-than-average SLP in the Arctic, together with a higher-than-average SLP over the mid-latitudes. Although the AO is defined using SLP, it is also a signature of the strength of the Stratospheric Polar Vortex (SPW), with AO+ linked to strong, and AO– to weak SPW (Baldwin and Dunkerton, 1999; Thompson and Wallace, 1998). In the current climate, the AO is strongly correlated with the NAO (Deser et al., 2000), but the patterns might become more distinguishable from each other in the future climate (Hamouda et al., 2021).

We used the daily Arctic Oscillation from the NOAA Climate Prediction Center (CPC). They calculated the AO by applying EOF on the monthly mean 1000hPa height anomalies at 20-90°N according to Thompson and Wallace (1998). The pressure fields were obtained from the NCEP/NCAR reanalysis dataset at a spatial resolution of 2.5°× 2.5°. The base period for their EOF analysis was 1979-2000 and they used the year-round monthly mean pressure fields from which the seasonal cycle had been removed.

2.3.2 Arctic Dipole Anomaly

We define the Arctic Dipole Anomaly (DA) as the second Principal Component (PC) of the EOF analysis of the SLP over the Central Arctic (latitudes 70-90°N) following Wu et al. (2006). The DA is characterized by a sea-level pressure dipole with the centres of action over the Barents-Kara Sea and Canadian Archipelago-Greenland region. These pressure patterns drive the Transpolar Drift Stream and sea ice export via the Fram Strait. Wu et al. (2006) calculated the DA index for the monthly means over the period of 1960-2002. Here, we applied the same method for winter (December to March) daily SLP values over our

https://doi.org/10.5194/egusphere-2026-1578
Preprint. Discussion started: 22 April 2026

study period 2000-2025 using the ERA5 daily mean MSLP values. We performed EOF analysis for latitudes 70-90 °N using the EOFS v1.4.0 package in Python (Dawson, 2016) . The EOF patterns of the first and second modes of variability correspond well to the AO-like and DA pressure patterns.

2.3.3 North Atlantic Oscillation and Pacific - North American Pattern

The NAO is the leading structure of variability in the Northern Hemisphere Atlantic Sector. A positive NAO roughly describes a situation where the Icelandic low is deeper than average and the Azores High is stronger than average. The PNA is the main structure of variability in the Pacific Sector. A positive phase PNA consists of a lower-than-average pressure over the Aleutian Islands and a higher-than-average pressure over western Canada. Deser et al., (2000) applied Rotated Principal Component Analysis to the 700mb geopotential height data from 15 to 90°N, which became the standard for solving the NAO and PNA. While the NAO is a primary pattern of variability in all seasons, the PNA is mostly a cold-season circulation structure. We used the NAO and PNA from the NOAA CPC. Daily values were calculated following Barnston and Livezey (1987).

2.4 Self-Organizing Maps

We identified and clustered the large-scale circulation types using the SOM method, which is a statistical unsupervised learning method for determining generalised patterns in data, developed by Kohonen (2001). SOM is a type of artificial neural network and hence a machine-learning approach.

We used the SOM method to allocate 12 (3×4) characteristic atmospheric winter (December–March) circulation types for 12/2000-3/2025. The input data were the mean sea-level pressure (MSLP) fields from the ERA5 reanalysis. We performed SOM analysis for the region north of 50°N, thus capturing the Icelandic and a sufficient part of Aleutian Lows, which are both essential centres of action for the NAO and PNA.

First, we re-gridded the input MSLP data to an equal-area grid (EASE2 with a 50 km × 50 km resolution). The actual SOM procedure included initialisation, training, evaluation, and visualisation. In this study, we applied a random initialisation scheme to create an initial SOM array, in which each node had an associated reference vector with dimensions equal to those of the input MSLP data. During training, each input data vector (i.e. each time step of the MSLP data) was compared with the reference vector of each node, and those reference vectors that were most similar to the input data vector were adjusted towards the input data vector. The training continued until the reference vectors converged. Consequently, an SOM array of characteristic MSLP patterns was obtained. In the final SOM array, the nodes are organised such that the most similar circulation patterns are located close to each other, while the most dissimilar patterns are situated in the corners of the array. Each time step of the input MSLP field was associated with the most similar node. The plots (Figure 1 and Figure 2) show composites of the MSLP fields from ERA5, and not the reference vectors directly from the SOM.

2.5 Transects for the ice motion analysis

We defined three transects in the Arctic to quantify the ice motion variations (locations are shown in Figure X). We selected locations in the Beaufort Gyre (BG), the Transpolar Drift Stream (TDS) and Fram Strait (FS), and calculated the average ice speed across those transects. We defined BG in the Southern Beaufort Sea (210°E; 71-74°N), TDS in the eastern central Arctic (60°E; 82-86°N), and FS between Greenland and Svalbard (350-7°E; 80°N). BG and TDS are defined along longitudes, and FS along latitude. Thus, to calculate the ice speed across the transect, we selected the zonal component for BG and TDS and the meridional component for FS. We decided on the location of the BG following Mallett et al., (2021) and TDS following Välisuo and Tietsche (2025), with minor modifications to the location. The FR transect is located between Greenland and Svalbard. We use a convention where the typical flow direction is positive: at BG, the flow from east to west is positive, and at TDS and FR, the flow towards the Atlantic is defined as positive.

https://doi.org/10.5194/egusphere-2026-1578
Preprint. Discussion started: 22 April 2026

3 Results

3.1 Atmospheric circulation types's assosiation with large scale circulation indices

Figure 1 shows the average MSLP for each circulation type ("SOM node"). The titles in the figure indicate the average duration of each circulation type and the proportion of cases belonging to each circulation type (occurrence %). We did not observe statistically significant trends in the occurrence of circulation types over our study period (2000-2025). The subplots are arranged according to the similarities between the circulation types. Towards the upper right corner, the circulation types show increasing cyclonic activity in the Atlantic region. The lower left corner shows the anticyclonic circulation in the central Arctic. We identified circulation types with low pressure in the Barents Sea region toward the lower right corner. Circulation types in the upper left corner are characterised by strong high pressure over Siberia.

Figure 2 shows the average MSLP anomaly for each circulation type and its association with the large-scale circulation indices (AO, NAO, DA, and PNA). We calculated the anomalies by comparing each time step of the MSLP to the climatology of 2000-2025. The features of the pressure fields are reflected in the average circulation index of each node. NAO increases towards the upper right corner of the panel plot, together with the decreasing average MSLP in the North Atlantic (Figure 1). NAO values decreased towards the lower left corner. AO, which is correlated with the NAO, behaves similarly. Circulation types towards the right represent a positive DA, and circulation type 9 had the highest DA value (1.22). Circulation types on the left had negative values for the DA, with Node 4 being the most negative (–1.43). The mean PNA also varies between the circulation types: we see positive PNA values when the Aleutian low is prominent, especially in Nodes 4, 5, 7, and 8.

https://doi.org/10.5194/egusphere-2026-1578
Preprint. Discussion started: 22 April 2026

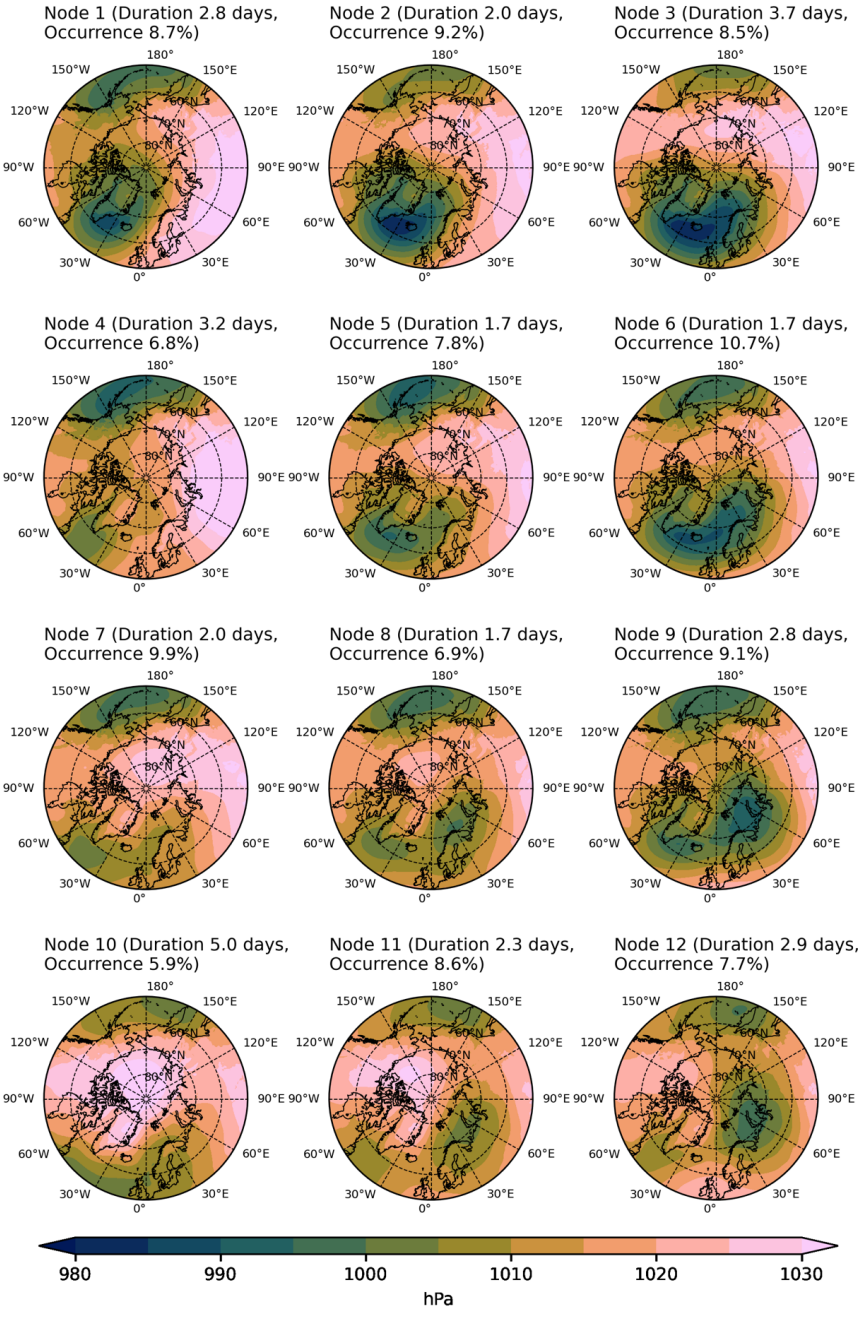

175 **Figure 1: Average mean sea level pressure in each circulation type, called SOM node, in winters (DJFM) of 2000-2025. The titles indicate the average duration of the circulation type, and the proportion of cases belonging the each circulation type (Occurrence %)**

https://doi.org/10.5194/egusphere-2026-1578
Preprint. Discussion started: 22 April 2026

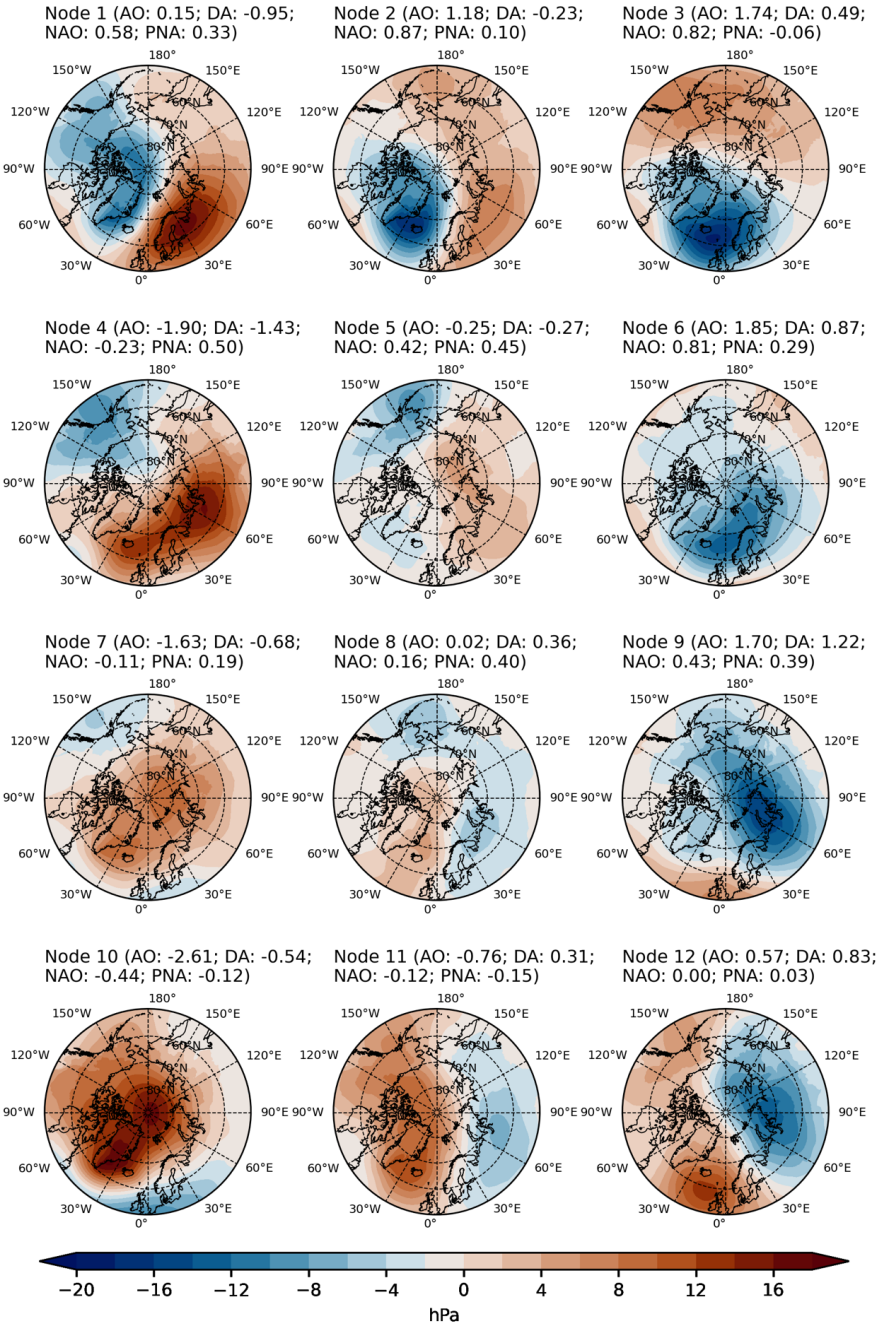

Figure 2: Average mean sea level pressure anomaly in each circulation type, called SOM node, in winters (DJFM) of 2000-2025. The titles show the average Arctic Oscillation (AO), Arctic Dipole Anomaly (DA), North Atlantic Oscillation (NAO), and Pacific North American Pattern (PNA) in the cases belonging to each node.

https://doi.org/10.5194/egusphere-2026-1578
Preprint. Discussion started: 22 April 2026

3.2 Ice drift speed's association with atmospheric circulation type

Figure 3 shows the average ice motion for each atmospheric circulation type. The values in the figure titles indicate the average ice drift speed across the transects in the Beaufort Gyre (BG), Transpolar Drift Stream (TDS), and Fram Strait (FR). The general ice motion in the Arctic is anticyclonic, reflecting the impact of the Beaufort Sea high pressure and the Atlantic and Aleutian low pressure systems in the ice drift. We observed that the ice drift speed across the transect can be over three times faster when the circulation type is favourable. For example, in Node 1, the average ice drift speed at BG was 2.0 km/d, compared to 7.1 km/d in Node 11. The Beaufort Sea high was absent in Node 1; thus, an essential driver of the BG was missing. Node 11, in contrast, had a well-defined Beaufort Sea high, centred in an optimal location to drive the ice across the Beaufort Sea transect.

https://doi.org/10.5194/egusphere-2026-1578
Preprint. Discussion started: 22 April 2026

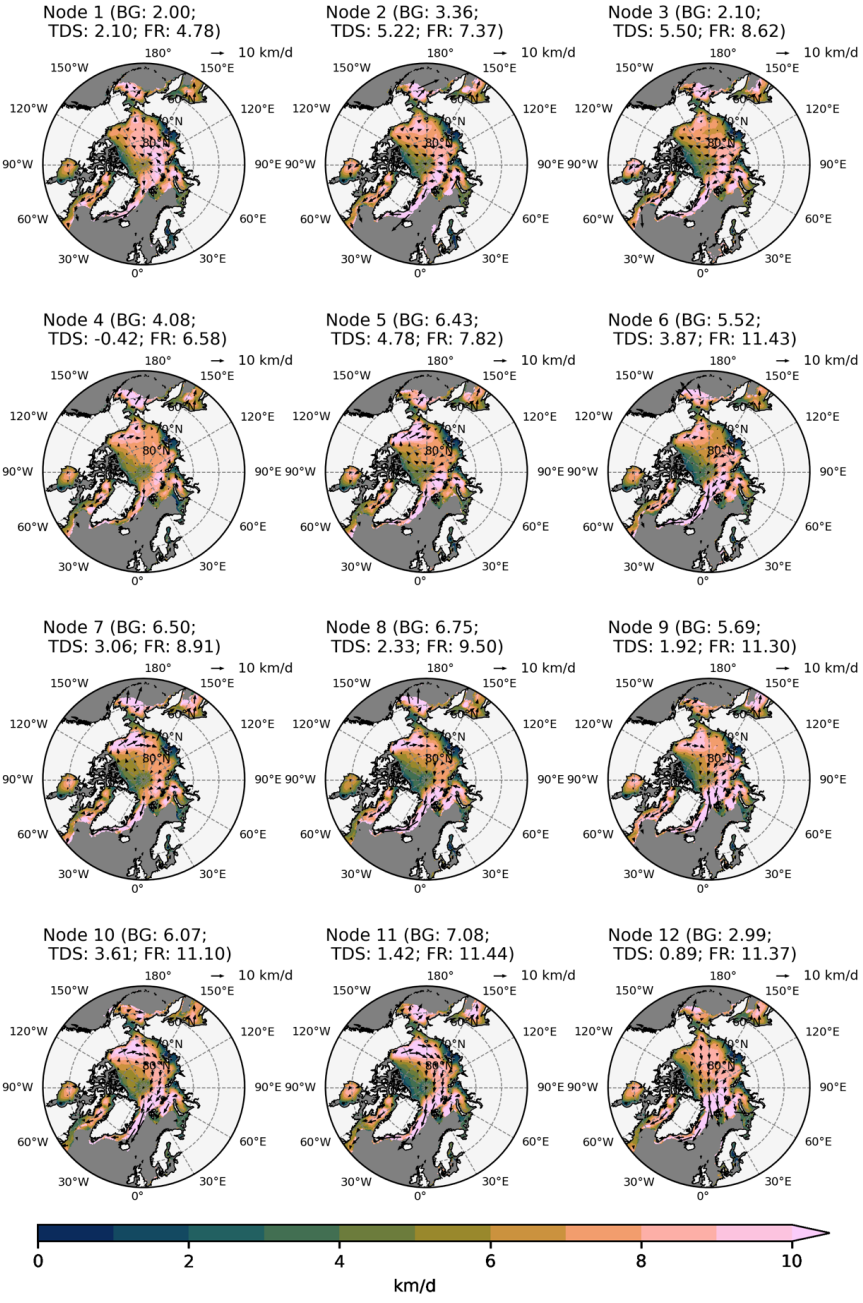

Figure 3: Average ice drift speed in each circulation type in winters 2000-2025. The titles tell the average ice drift speed across the Beaufort Gyre (BG), Transpolar Drift Stream (TDS), and Fram Strait (FR) -transects.

195

https://doi.org/10.5194/egusphere-2026-1578
Preprint. Discussion started: 22 April 2026

In Figure 4, we identify the pressure systems that are the most essential drivers of ice speed in the BG, TDS, and FR. The plots in Figure 4 show the spatial correlation between the ice drift speed across the transect and the MSLP. We calculated the correlations based on the daily values of the ERA5 MSLP and Polar Pathfinder ice motion data. Correlations were calculated for winters (DJFM) 2000-2023, as the Polar Pathfinder dataset covers years until the end of 2023. There were two main centres of action associated with the sea ice drift speed at each transect. The approximate locations of these centres of action are listed in Table 1 for use in the regression analysis (Figure 5). The ice velocity at the BG transect was negatively correlated with air pressure at the Bering Strait and positively correlated with sea level pressure over the Beaufort Sea. In other words, a low pressure in the Bering Strait region and high pressure centred over the Beaufort Sea are linked to strong eastward ice drift in the southern Beaufort Gyre. In the case of the TDS, the signs of the correlation coefficient suggest that a high-pressure in the eastern central Arctic and low pressure in the Svalbard-Barents Sea region are associated with increased ice speeds towards the Atlantic. Unlike the other two transects, the TDS is not confined by any geographic barrier, thus defining a fixed location for the TDS transect is arbitrary. The location of the TDS fluctuates according to the pressure systems that drive the flow. To complement the TDS results, we defined the third transect in the Fram Strait (FR). The southward ice drift in the Fram Strait can be interpreted as the final part of the TDS. However, we identified that the pressure patterns driving the ice motion were not identical for the TDS and FR, and the ice drift speed in the TDS was not clearly related to the drift speed in the FR (Figure 5). The MSLP patterns essential for the southward ice drift in FR are high pressure over the Canadian Archipelago and low pressure over the Barents Sea. Tsukernik et al. (2010) presented an almost identical correlation map in their analysis of the drivers of Fram Strait ice flow.

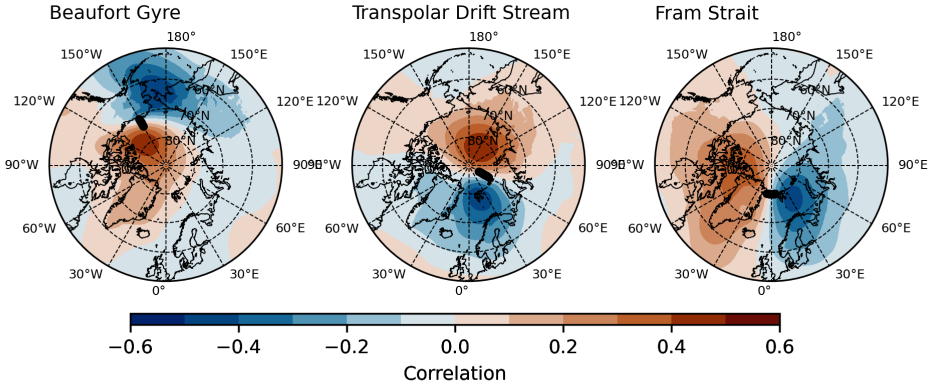

Figure 4: Correlations of mean sea level pressure and sea ice drift speed across the Beaufort Gyre, Transpolar Drift Stream and Fram Strait transects in winters (DJFM) 2000-2025. The locations of the transects are show in the plots with the thick black line.

	High	Low
BG	-145E; 80N	-170E; 65N
TDS	150E; 83N	20E; 78N
FR	-90E; 78N	30E; 76N

Table 1: Location of the MLSP centres of action that drive the ice drift across the transects.

https://doi.org/10.5194/egusphere-2026-1578
Preprint. Discussion started: 22 April 2026

The heatmaps in Figure 5 show the average drift speed across each transect in each SOM-node, and the average MSLP gradient along the transect. We calculated the MSLP gradient between the two centres of action identified in Figure 4 and Table 1. Faster drift speed was associated with stronger MSLP gradient, which causes a stronger geostrophic wind that drives the ice motion. While the correlation maps identify two centres of action that drive the ice flow in each location, the results show that either a strong low pressure on the left-hand side or a strong high pressure on the right-hand side is sufficient to increase the drift speed.

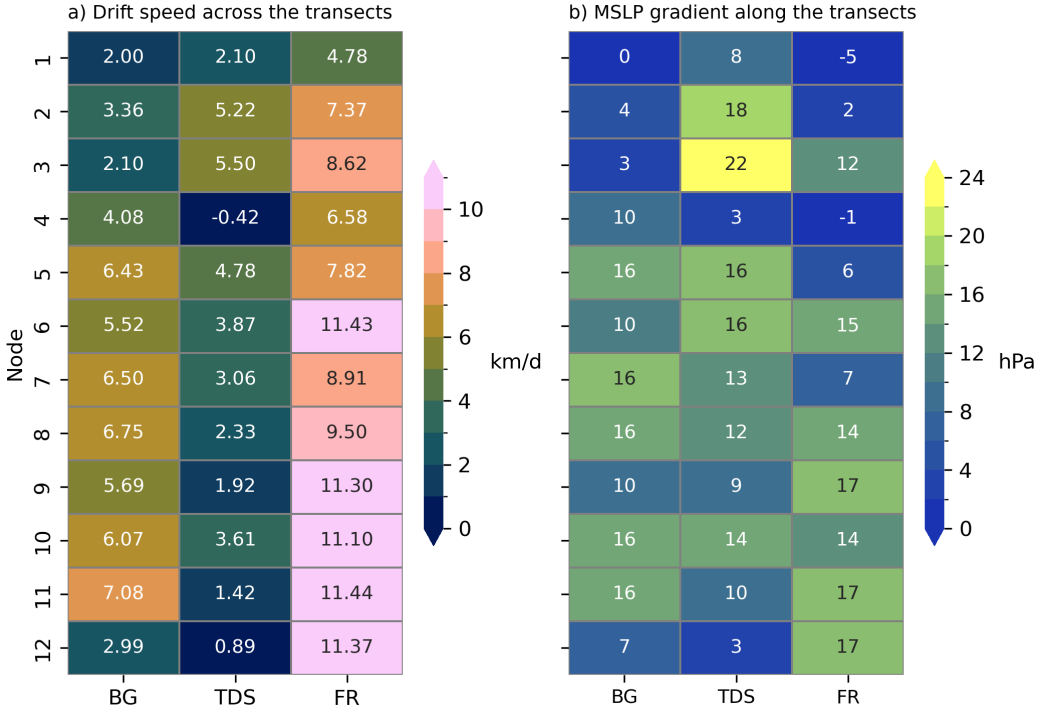

Figure 5: a) Average ice drift speed across each transect in each node, and b) the corresponding Mean Sea Level Pressure (MSLP) gradient along the transect. The MSLP gradient is calculated for each transect based on the two points that are defined in Table 1. BG refers to Beaufort Gyre, TDS to the Transpolar Drift Stream and FR to Fram Strait.

At BG the drift speed exceeded 6 km/d in nodes 5, 7, 8, 10 and 11. In node 5 the dominant driver was the negative MSLP anomaly over the Aleutian Archipelago (Figure 1 and Figure 2). Nodes 7 and 8 were impacted by a negative MSLP anomaly in the Aleutian region and a positive anomaly in the central Arctic. In nodes 10 and 11, the pressure gradient was caused by a stronger that average high pressure in the Arctic. In these five circulation types, the AO values ranged from –2.61 to 0.02 (nodes 10 and 8, respectively), NAO from –0.44 to 0.42 (nodes 10 and 5, respectively), PNA from –0.15 to 0.45 (nodes 11 and 5, respectively), and DA from –0.68 to 0.36 (nodes 7 and 8, respectively).

At TDS we observed fastest drift speeds in nodes 2, 3, 5 and 6. In nodes 2 and 3 strong Islandic low pressure and moderate positive pressure anomalies over the Siberian or Pacific Arctic contributed to the fast ice drift. In nodes 2 and 3, the AO and NAO indices were positive. In node 5 the AO index was negative and the NAO index was positive. There was a moderate positive pressure anomaly over the Laptev and East Siberian Seas and a weak low pressure anomaly over Iceland and southern Greenland. We interpret that pressure gradient between Siberian Seas and Iceland was the main contributor to the fast drift speed in TDS in node 5. In node 6 the MSLP gradient was the same as in node 5, but the drift speed across TDS transect was

https://doi.org/10.5194/egusphere-2026-1578
Preprint. Discussion started: 22 April 2026

lower (4.8 km/d vs. 3.9 km/d). The MSLP field was dominated by a negative anomaly in the northern Atlantic, which seemed the main driver of increase drift speed.

Ice drift speed at the FR transect is clearly associated with the SOM nodes. Nodes 6, 9, 10, 11 and 12 showed the fastest drift speeds. The increased drift speed was associated with the pressure gradient between the left- and right-hand side of the flow. Almost all fast ice drift nodes had a low pressure over the Barents Sea. This was missing only in node 10, where the necessary pressure gradient was caused by a high pressure over Greenland alone.

We built linear regression models to quantify the relationship between ice drift speed and atmospheric pressure. First, we formed linear regression models where the explanatory variable (y) is the ice drift speed across a transect, and the explaining variables (X) are the large-scale circulation indices NAO, AO, DA, and PNA. In our results, the variations in the large-scale circulation indices explained less than 15% of the variations in ice drift speed (Figure 5, upper row). Second, we formed linear regression models between the ice drift speed and mean sea level pressure at the centres of action identified in the correlation maps (Figure 4) and Table 1. Using the MSLP from the location where the correlation with the ice drift speed was highest, we reached explanation levels of 40% to 62% (Figure 5, lower row). We interpret the results such that the variations in MSLP explain approximately 50% of the ice drift speed variations, and the exact locations of the cyclones and anticyclones are essential for the drift speed and direction. This is in line with the rule of thumb that the geostrophic wind explains approximately 50% of the ice drift speed variability (Colony and Thorndike, 1984). The large-scale circulation indices do not describe the local features of the pressure field, which makes them poor explainers of ice drift in specific locations, such as the transects that we used in this study.

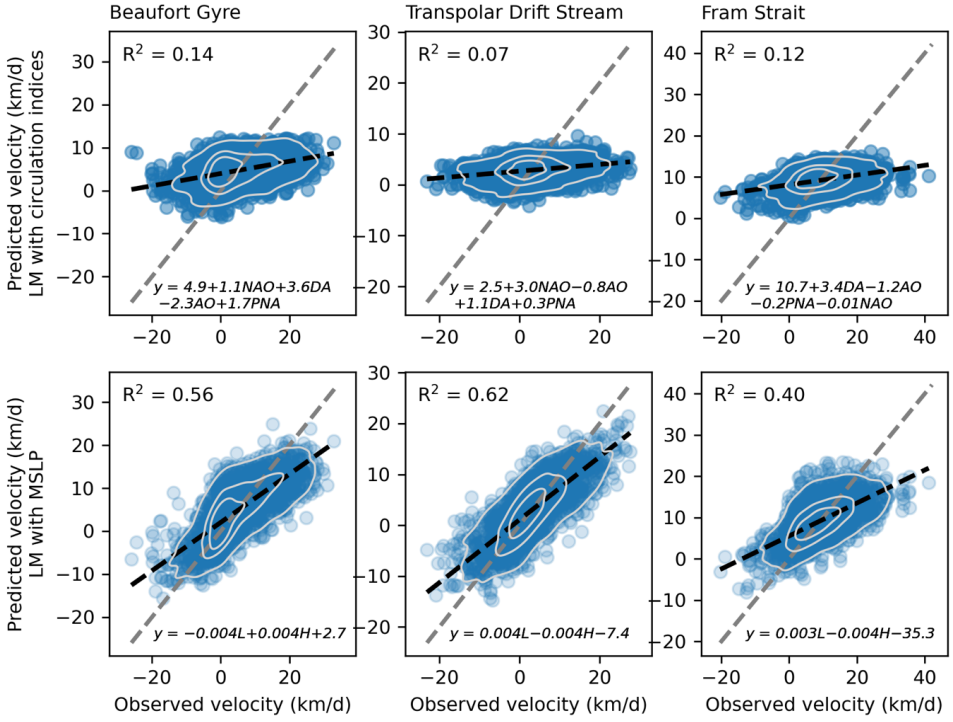

Figure 6: Linear regression models (LM) for ice velocity across the three transects. The upper row shows the multi-linear regression models based on the large-scale circulation indices: North Atlantic Oscillation (NAO), Arctic Oscillation (AO), Arctic Dipole Anomaly (DA), and Pacific-North American Pattern (PNA). The lower row shows the regression models, where the explaining variables are the mean sea level pressure at the low pressure (L) and high pressure (H) centres of action, which are identified in the correlation maps in Figure 4.

https://doi.org/10.5194/egusphere-2026-1578
Preprint. Discussion started: 22 April 2026

4 Discussion and conclusions

The atmospheric pressure affects ice drift location, direction and velocity of the ice. There are climatological pressure patterns, that create semi-permanent ice drift features such as the TDS and BG, in the Arctic. Here, we studied ice drift speed at fixed locations. We investigated what atmospheric pressure patterns drive the ice drift in these locations. This is a suitable approach, when the drift patterns are rather constant. The ice drift in the BG and FR are contained by the vicinity of the coast, while TDS has no limiting geographic boundaries, and has a more variable location and direction. An optimal method for studying the atmosphere—drift speed interactions could be tracking the most prominent ice drift features at the same time with the location and intensity of the atmospheric pressure patterns.

At all the three transects the increased drift speed was connected to regional MSLP patterns rather that any large-scale circulation index. The large-scale circulation indices are defined as leading components of atmospheric variability of almost the whole hemisphere (e.g. 20-90°N for AO, and 15-90°N for NAO). The leading components are only partly linked to the pressure features that define the ice drift patterns in the Arctic. For example the Icelandic low pressure, a typical features of NAO+, is linked to increased ice export via the Fram strait, but the most essential MSLP patterns for the FR are the Barents Sea low pressure and Greenland high pressure. Further, the same large-scale indices foster varying regional MSLP patterns. In our results nodes 3 and 9 have almost the same AO index (1.74 and 1.70, respectively), the intensity of the Barents sea low pressure and Beaufort Sea high pressure are different, as is their signature on the ice drift speed.

In Figure 4 we identified for each transect two MSLP centres of action that correlated with the ice drift speed. Analysing the circulation types (Figure 1) more closely, we saw that a pressure dipole was not necessary to drive the fast flow. Instead, either a high-pressure anomaly on the right-hand side of the drift direction or a low-pressure anomaly on the left-hand side was sufficient to produce a positive ice drift anomaly, as the resulting pressure gradient drives a geostrophic wind that accelerates the sea ice. A key feature in the system is the anticyclone centred in the western central Arctic, often referred to as the Beaufort Sea High (BSH)(Serreze and Barrett, 2011). The BSH has been seen as a signature of the AO (Rigor et al., 2002), too. When the BSH is positioned in the western central Arctic, it favours the classic anticyclonic BG and supports the transport of ice from the Siberian coast toward the TDS (eg. Colony and Thorndike, 1984). In our results the strength and location of the BSH drives and modulates both BG and TDS. In Figure 4, a west-centred BSH is linked to strengthened BG and an east-centred BSH to stronger TDS. The pole-, and eastward shift of the BSH centre is associated with expectational Arctic Sea ice export in winter 2020/2021 in a study by Mallett et al. (2021). Further, low MSLP over the Barents Sea contributed to fast ice drift in the TDS and intensive ice export in the Fram Strait. Climate change has reduced the winter sea ice cover in the Barents Sea, creating a pathway for increased cyclonicity in the region, that favours sea ice export from the Arctic. The positive feedback loop on Barents Sea warming has been suggested by e.g. Smedsrud et al., (2013)

Large-scale circulation indices explain less than 15% of the variation in local drift speed, indicating that these indices are not reliable proxies for ice drift speed. To enhance the analysis, self-organizing map (SOM) techniques can be applied, revealing that high drift speeds in the Fram Strait (FR) occurred not only in nodes with strong dipole anomalies (DA) but also in nodes where either centre of action is pronounced, such as nodes 10 and 11. Furthermore, since the location of the Transpolar Drift Stream (TDS) is not constrained by any coastline, both its position and drift speed are highly sensitive to atmospheric pressure patterns.

Drift speed at TDS was especially poorly linked to large scale circulation indices, but the correlation between the local MSLP and drift speed was highest of all our three locations. There are several possible reasons for this. First, the large scale circulation indices that we studies do not describe the MSLP dipole that drives the ice drift in the TDS across the Arctic. The AO– and NAO+ circulation feature a positive pressure anomaly in the central Arctic, but lack the negative pressure anomaly over

https://doi.org/10.5194/egusphere-2026-1578
Preprint. Discussion started: 22 April 2026

Svalbard (Figure 4 b). Also, AO– is linked to the pressure anomaly over the whole Arctic, thus a low pressure in the Svalbard region might decrease the AO-index. Furthermore, we defined the TDS as a drift pattern that brings ice towards the Fram Strait and the Atlantic Ocean. We observed also cases, where the TDS was almost reversed: ice motion in the Arctic was intensive, but the location and direction did not match our definition of TDS.

Taken together, our results show that the ice drift at all three transects responds primarily to regional MSLP patterns rather than to any large-scale circulation index. The AO and NAO capture only a portion of the pressure variability relevant for Arctic ice motion, and therefore explain only a small fraction of the drift speed changes. In contrast, the SOM analysis highlights the specific pressure anomalies that drive enhanced drift, and illustrates how their location relative to the flow is essential, especially for the unconstrained TDS. The strong sensitivity of the TDS drift speed to local pressure features, together with its variable position, emphasizes the need for approaches that follow the dominant drift pathways and their associated pressure structures simultaneously. Such methods would provide a more robust framework for understanding how changing atmospheric patterns shape the Arctic ice drift under present and future climate conditions.

Code and data availability

This study is based on open data that can be access via the following sources:

ERA5: Copernicus Climate Change Service, Climate Data Store, (2023): ERA5 hourly data on single levels from 1940 to present. Copernicus Climate Change Service (C3S) Climate Data Store (CDS). DOI: 10.24381/cds.adbb2d47. [Accessed on several days Mar-2025].

Polar Pathfinder: Tschudi, M., W. N. Meier, J. S. Stewart, C. Fowler, and J. Maslanik. 2019. Polar Pathfinder Daily 25km EASE-Grid Sea Ice Motion Vectors, Version 4. Boulder, Colorado USA. NASA National Snow and Ice Data Center Distributed Active Archive Center. https://doi.org/10.5067/INAWUWO7QH7B. [Accessed May 2025].

Large scale circulation indices:

NAO, AO, PNA circulation indices: NOAA Climate Prediction Center (CPC), https://ftp.cpc.ncep.noaa.gov/cwlinks/ , [Accessed May 2025].

A code repository to reproduce the data and the figures is in preparation and will be made accessible upon publication.

Author contributions

I.V. is responsible for planning of the study, preforming the final SOM-analysis, analysis the results, plotting the figures and writing the text. T.N. is responsible for planning and preforming an initial SOM-analysis, writing the SOM-method description text in section 2.4, reviewing and giving feedback on the results, figures and text.

Competing interests

The authors declare that they have no conflict of interest.

Financial support

I.V's contribution was supported by the Research Council of Finland through the project "Understanding the sub-seasonal to seasonal predictability of Arctic sea ice.", agreement number 339409.

https://doi.org/10.5194/egusphere-2026-1578
Preprint. Discussion started: 22 April 2026

References

Armitage, T.W.K., Bacon, S., Kwok, R., 2018. Arctic Sea Level and Surface Circulation Response to the Arctic Oscillation. Geophys. Res. Lett. 45, 6576–6584. https://doi.org/10.1029/2018GL078386

Baldwin, M.P., Dunkerton, T.J., 1999. Propagation of the Arctic Oscillation from the stratosphere to the troposphere. J. Geophys. Res. Atmospheres 104, 30937–30946. https://doi.org/10.1029/1999JD900445

Barnston, A.G., Livezey, R.E., 1987. Classification, Seasonality and Persistence of Low-Frequency Atmospheric Circulation Patterns. Mon. Weather Rev. 115, 1083–1126. https://doi.org/10.1175/1520-0493(1987)115%253C1083:CSAPOL%253E2.0.CO;2

Colony, R., Thorndike, A.S., 1984. An estimate of the mean field of Arctic sea ice motion. J. Geophys. Res. Oceans 89, 10623–10629. https://doi.org/10.1029/JC089iC06p10623

Dawson, A., 2016. eofs: A Library for EOF Analysis of Meteorological, Oceanographic, and Climate Data. J. Open Res. Softw. 4. https://doi.org/10.5334/jors.122

Deser, C., Walsh, J.E., Timlin, M.S., 2000. Arctic Sea Ice Variability in the Context of Recent Atmospheric Circulation Trends. J. Clim. 13, 617–633. https://doi.org/10.1175/1520-0442(2000)013%253C0617:ASIVIT%253E2.0.CO;2

Guemas, V., Blanchard-Wrigglesworth, E., Fučkar, N.S., Germe, A., Hawkins, E., Keeley, S., Koenigk, T., Salas y Mélia, D., Tietsche, S., 2014. A review on Arctic sea-ice predictability and prediction on seasonal to decadal time-scales. Q. J. R. Meteorol. Soc. 142, 546–561. https://doi.org/10.1002/qj.2401

Hamouda, M.E., Pasquero, C., Tziperman, E., 2021. Decoupling of the Arctic Oscillation and North Atlantic Oscillation in a warmer climate. Nat. Clim. Change 11, 137–142. https://doi.org/10.1038/s41558-020-00966-8

Hersbach, H., Bell, B., Berrisford, P., Hirahara, S., Horányi, A., Muñoz-Sabater, J., Nicolas, J., Peubey, C., Radu, R., Schepers, D., Simmons, A., Soci, C., Abdalla, S., Abellan, X., Balsamo, G., Bechtold, P., Biavati, G., Bidlot, J., Bonavita, M., De Chiara, G., Dahlgren, P., Dee, D., Diamantakis, M., Dragani, R., Flemming, J., Forbes, R., Fuentes, M., Geer, A., Haimberger, L., Healy, S., Hogan, R.J., Hólm, E., Janisková, M., Keeley, S., Laloyaux, P., Lopez, P., Lupu, C., Radnoti, G., de Rosnay, P., Rozum, I., Vamborg, F., Villaume, S., Thépaut, J.-N., 2020. The ERA5 global reanalysis. Q. J. R. Meteorol. Soc. 146, 1999–2049. https://doi.org/10.1002/qj.3803

Heukamp, F.O., Aue, L., Wang, Q., Ionita, M., Kanzow, T., Wekerle, C., Rinke, A., 2023. Cyclones modulate the control of the North Atlantic Oscillation on transports into the Barents Sea. Commun. Earth Environ. 4, 324. https://doi.org/10.1038/s43247-023-00985-1

Hordoir, R., Jahanmard, V., Isachsen, P.E., Löptien, U., Dietze, H., Sandø, A.B., Lien, V.S., 2026. Barents Sea atlantification driven by a shift in atmospheric synoptic timescale. Nat. Clim. Change 16, 179–186. https://doi.org/10.1038/s41558-025-02535-3

Kwok, R., Rothrock, D.A., 1999. Variability of Fram Strait ice flux and North Atlantic Oscillation. J. Geophys. Res. Oceans 104, 5177–5189. https://doi.org/10.1029/1998JC900103

Mallett, R.D.C., Stroeve, J.C., Cornish, S.B., Crawford, A.D., Lukovich, J.V., Serreze, M.C., Barrett, A.P., Meier, W.N., Heorton, H.D.B.S., Tsamados, M., 2021. Record winter winds in 2020/21 drove exceptional Arctic sea ice transport. Commun. Earth Environ. 2, 1–6. https://doi.org/10.1038/s43247-021-00221-8

Meredith, M., Sommerkorn, M., Cassotta, S., Derksen, C., Ekaykin, A., Hollowed, A., Kofinas, G., Mackintosh, A., Melbourne-Thomas, J., Muelbert, M.M.C., Ottersen, G., Pritchard, H., Schuur, E.A.G., 2019. Polar Regions, in: Pörtner, H.-O., Roberts, D.C., Masson-Delmotte, V., Zhai, P., Tignor, M., Poloczanska, E., Mintenbeck, K., Alegría, A., Nicolai, M., Okem, A., Petzold, J., Rama, B., Weyer, N.M. (Eds.), IPCC Special Report on the Ocean and Cryosphere in a Changing Climate. Cambridge University Press, Cambridge, UK and New York, NY, USA, pp. 203–320. https://doi.org/10.1017/9781009157964.005

Nicolaus, M., Perovich, D.K., Spreen, G., Granskog, M.A., von Albedyll, L., Angelopoulos, M., Anhaus, P., Arndt, S., Belter, H.J., Bessonov, V., Birnbaum, G., Brauchle, J., Calmer, R., Cardellach, E., Cheng, B., Clemens-Sewall, D., Dadic, R., Damm, E., de Boer, G., Demir, O., Dethloff, K., Divine, D.V., Fong, A.A., Fons, S., Frey, M.M., Fuchs, N., Gabarró, C., Gerland, S., Goessling, H.F., Gradinger, R., Haapala, J., Haas, C., Hamilton, J., Hannula, H.-R., Hendricks, S., Herber, A., Heuzé, C., Hoppmann, M., Høyland, K.V., Huntemann, M., Hutchings, J.K., Hwang, B., Itkin, P., Jacobi, H.-W., Jaggi, M., Jutila, A., Kaleschke, L., Katlein, C., Kolabutin, N., Krampe, D., Kristensen, S.S., Krumpen, T., Kurtz, N., Lampert, A., Lange, B.A., Lei, R., Light, B., Linhardt, F., Liston, G.E., Loose, B., Macfarlane, A.R., Mahmud, M., Matero, I.O., Maus, S., Morgenstern, A., Naderpour, R., Nandan, V., Niubom, A., Oggier, M., Oppelt, N., Pätzold, F., Perron, C., Petrovsky, T., Pirazzini, R., Polashenski, C., Rabe, B., Raphael, I.A., Regnery, J., Rex, M., Ricker, R., Riemann-Campe, K., Rinke, A., Rohde, J., Salganik, E., Scharien, R.K., Schiller, M., Schneebeli, M., Semmling, M., Shimanchuk, E., Shupe, M.D., Smith, M.M., Smolyanitsky, V., Sokolov, V., Stanton, T., Stroeve, J., Thielke, L., Timofeeva, A., Tonboe, R.T., Tavri, A., Tsamados, M., Wagner, D.N., Watkins, D., Webster, M., Wendisch, M., 2022. Overview of the MOSAiC expedition: Snow and sea ice. Elem. Sci. Anthr. 10, 000046. https://doi.org/10.1525/elementa.2021.000046

Nygård, T., Papritz, L., Naakka, T., Vihma, T., 2023. Cold wintertime air masses over Europe: where do they come from and how do they form? Weather Clim. Dyn. 4, 943–961. https://doi.org/10.5194/wcd-4-943-2023

Olason, E., Notz, D., 2014. Drivers of variability in Arctic sea-ice drift speed. J. Geophys. Res. Oceans 119, 5755–5775. https://doi.org/10.1002/2014JC009897

Perovich, D.K., Polashenski, C., 2012. Albedo evolution of seasonal Arctic sea ice. Geophys. Res. Lett. 39. https://doi.org/10.1029/2012GL051432

https://doi.org/10.5194/egusphere-2026-1578
Preprint. Discussion started: 22 April 2026

Rigor, I.G., Wallace, J.M., Colony, R.L., 2002. Response of Sea Ice to the Arctic Oscillation. J. Clim. 15, 2648–2663. https://doi.org/10.1175/1520-0442(2002)015%253C2648:ROSITT%253E2.0.CO;2

Serreze, M.C., Barrett, A.P., 2011. Characteristics of the Beaufort Sea High. J. Clim. 24, 159–182. https://doi.org/10.1175/2010JCLI3636.1

Smedsrud, L.H., Esau, I., Ingvaldsen, R.B., Eldevik, T., Haugan, P.M., Li, C., Lien, V.S., Olsen, A., Omar, A.M., Otterå, O.H., Risebrobakken, B., Sandø, A.B., Semenov, V.A., Sorokina, S.A., 2013. The Role of the Barents Sea in the Arctic Climate System. Rev. Geophys. 51, 415–449. https://doi.org/10.1002/rog.20017

Thompson, D.W.J., Wallace, J.M., 1998. The Arctic oscillation signature in the wintertime geopotential height and temperature fields. Geophys. Res. Lett. 25, 1297–1300. https://doi.org/10.1029/98GL00950

Tschudi, M., Meier, W.N., Stewart, J.S., Fowler, C., Maslanik, J., 2019. Polar Pathfinder Daily 25 km EASE-Grid Sea Ice Motion Vectors. https://doi.org/10.5067/INAWUWO7QH7B

Tsukernik, M., Deser, C., Alexander, M., Tomas, R., 2010. Atmospheric forcing of Fram Strait sea ice export: a closer look. Clim. Dyn. 35, 1349–1360. https://doi.org/10.1007/s00382-009-0647-z

Välisuo, I., Tietsche, S., 2025. Forecasting Arctic sea-ice drift: insights from two case studies. Ann. Glaciol. 66, e7. https://doi.org/10.1017/aog.2024.48

Vihma, T., Tisler, P., Uotila, P., 2012. Atmospheric forcing on the drift of Arctic sea ice in 1989–2009. Geophys. Res. Lett. 39. https://doi.org/10.1029/2011GL050118

Wilks, D.S., 2011. Statistical Methods in the Atmospheric Sciences. Academic Press.

Wu, B., Wang, J., Walsh, J.E., 2006. Dipole Anomaly in the Winter Arctic Atmosphere and Its Association with Sea Ice Motion. J. Clim. 19, 210–225. https://doi.org/10.1175/JCLI3619.1